3.1 Introduction

Investigation on gel-like soft resources has been emerging curiously because of their massive applications extending from researchers to manufacturing areas[1,2]. Supramolecular gels have potential capabilities over several fields including catalysis[1], lithography[2,3], optoelectronic devices[3], electrochemical devices[4], chemo-sensors[5], cell culturing[5], biomedicine[6,7], medical diagnostics[7], drug delivery[8,9], wastewater treatment[10], tissue engineering[9], sensor science[11], and semiconductor[12]. During the last two decades, the discovery of a new low molecular weight conducting metallogelator has been accompanied by a decisive development in the field of coordination polymer and metal-organic framework that may build up novel metallogel with challenging features[13]. In recent research, conductive metallogels have turned out to be a captivating functionalized material[14] because of their advancement in optical, electronics, and electrical devices[15]. However, synthesis of conductive metallogel, having self-healing property to fabricate electronic devices, is still a challenging task in a scientific community[11]. Metal–semiconductor (MS) junctions are a crucial part of effectively all the semiconducting optoelectronic devices[16]. The formation of this MS junction interface sturdily affects the quality and performance of the devices[17]. During the last few years, there has been considerable attention on the experimental studies of MS-based Schottky Barrier diodes (SBDs). The present disclosure generally relates to SBDs that have a metal for the Schottky layer and the semiconductor material for the drift layer is selected to provide a low barrier height Schottky junction between the drift layer and the Schottky layer. Schottky-Barrier height (SBH) is a key property of MS interface of SBDs, which governs the electronic carriage across the interface[18], and the electrical characterisation such as voltage drop and

switching speed of such devices is dependent on the current transport behaviour through the structure of the MS interface. The SBDs provide great advantages over a traditional analogous p-n diode as they have lesser barrier height; thus, it is required to lower Voltage to turn on the device[19].

Taking all these into consideration, we have examined the semiconducting properties of synthesized metallogel (Cu-H_4L) and successfully fabricated a metal-semiconductor junction-based thin-film device (Ag/Cu-H_4L) at room temperature (RT). The calculated direct energy band gap of metallogel was ~3.06 eV, which showed the improved optical properties to that of previously reported literature[12,20]. The *I-V* characteristics of the Ag/Cu-H_4L based thin-film device display a nonlinear rectifying behaviour, suggesting the formation of a Schottky Barrier diode. The imperative SBDs parameters of the fabricated device such as rectification ratio, ideality factor, and Barrier height were extracted from current-voltage characteristics by Cheung's method. It is, therefore, of critical importance to reduce the barrier height of the Ag/Cu-H_4L interface to improve the on-state voltage drop in Ag/Cu-H_4L devices. Moreover, it has also been extensively studied that our designed semiconducting thin-film based SBD has the advantages of enhanced electrical conductivity, high chemical stability and a low-cost production process.

3.2 Materials

Succinic acid, Hydrazine hydrate, salicylaldehyde, copper acetate monohydrate, and solvents were acquired from S.D. Fine Private Ltd. Throughout the whole experiments, the chemicals were used without additional purification.

3.3 Characterization

The UV-vis spectra were conducted on a Thermo Scientific EVOLUTION 201 characterization. ^{1}H NMR study was conducted by Bruker AVANCE III HD 500 spectrometer. Micromass MS Technologies SCIEX X500R QTOF was used for recording the HR-MS spectra. Tecnai G2 20 TWIN was used for capturing TEM micrographs. Rheology of metallogel was achieved on Anton Paar MCR 702 Twin Drive Rheometer. The SEM images were collected on EVO-Scanning Electron Microscope MA15/18. Powder XRD data was accumulated in the range of angle $2\theta = 10 \square 90^{o}$ on Rigaku MiniFlex 600 Detector D-tex ultra.

3.4.1 Synthesis of gelator (H_4L)

The reported ligand[18] was synthesized by the reaction mixture of methanolic solution of succinic acid (1.00g, 8.46 mmol) and a catalytic amount of concentrated sulphuric acid was refluxed overnight. Afterward, a clear solution of dimethyl succinate was obtained with a pleasant smell. Further, this methanolic mixture was refluxed with hydrazine hydrate (863 mg, 16.9 mmol) under the in-situ condition for 6 hours, leads to the white crystals of succinoyldihydrazine, which was isolated by filtration. Then, dihydrazone was prepared by reacting a solution of succinoyldihydrazine (1.0 g, 6.8 mmol) with salicylaldehyde in methanol (1.67 g, 13.6 mmol). Subsequently, a white precipitate was obtained at RT, which was dried and collected after washing with methanol, resulting in the yield of 82% of H_4L gelator.

^{1}H NMR of synthesized gelator was conducted in [D_6] DMSO. ^{1}H NMR (500 MHz, [D_6] DMSO, 25 °C): δ = 11.72 (s, 1 H, -OH); 11.29 (s, 1 H, -OH); 11.17 (s, 1 H, NH); 10.15 (s, 1 H, NH); 8.35 (s, 1 H, CH=N); 8.28 (s, 1 H, CH=N); 6.85-7.65 (m, 8H, Ar-H); 2.93 (m, 2 H); 2.50 (m, 2 H).

3.4.2 Gelation ability test

The gelation ability of various metal cations with gelator H_4L was tested in DMF, and maintaining the minimum critical gel concentration of Cu-H_4L metallogel from the synthetic method of metallogel, described in the experimental section. The gel formation strategy of Cu-H_4L metallogel in different solvents were also checked by 'inversion of the vial' test. it was clearly revealed that the $Cu(OAc)_2 \cdot H_2O$ and gelator H_4L based mechanically stable Cu-H_4L metallogel can exclusively form in DMF

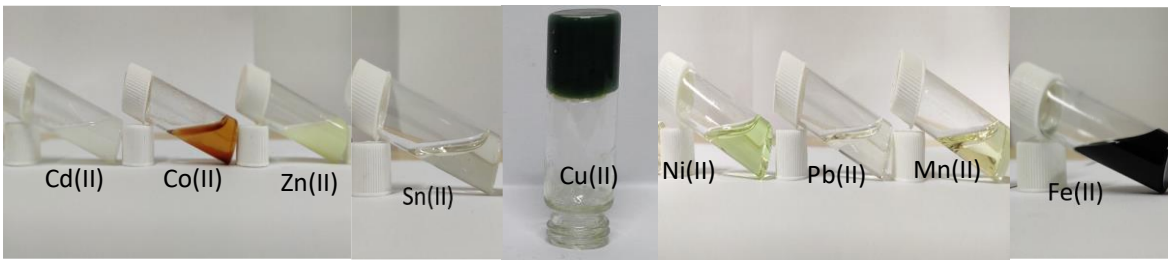

Figure 3.1. Gelation ability test of metal cations with gelator H_4L in DMF.

3.5 Synthesis of metallogel

In a typical synthesis process, the gelator H_4L (14 mg, 0.04 mmol) was dissolved in DMF (0.6 mL) in a vial. Then a freshly prepared $Cu(OAc)_2$ (8.0 mg, 0.04 mmol) solution in DMF (0.4 mL) was added in one shot. A green colour stiff gel was formed instantly at RT without any external mechanical influence. Thus, formed gelatinous material was examined by conventional inverted vial method, which confirmed the sustainability of the gel.

3.6 Device fabrication

For metal-semiconductor (MS) junction device fabrication, an Indium doped Tin oxide (ITO) coated glass substrates (15×15 mm^2) are ultrasonically cleaned using standard wet cleaning subsequently in the soap solution for 20 minutes, deionized (DI) water for 15 minutes, acetone

10 minutes, and isopropanol for 10 minutes and finally treated by plasma cleaning in the presence of argon for 20 minutes.[19,20] Initially, supramolecular Cu-based metallogel was deposited on the ITO coated glass substrate and annealed at 100^0C for 30 min. In the second step, ~80 nm thickness of metal (Ag) was deposited for a contact electrode by using a thermal evaporator unit. The evaporated metal (Ag) form the circular dots of a 1 mm radius on the top of the semiconductor device using a shadow mask technique[20]. The thicknesses of the Cu-H4L gel layer (~200 nm) were measured using the F20 Filmmetrics, USA instrument.[20]

3.7 Result and discussion

To synthesize metallogel, first, we have designed the gelator (H_4L), derived from succinic

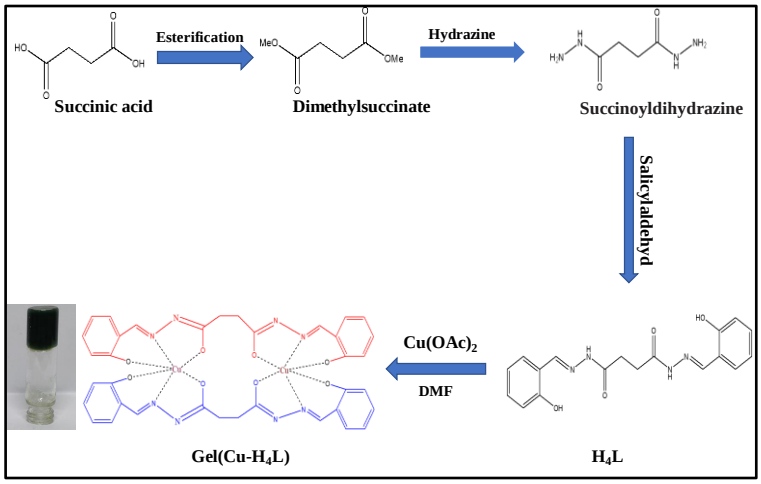

Scheme 3.1 Synthetic scheme of Cu-H_4L based metallogel.

acid, as shown in **Scheme 3.1.** The direct gelation test was performed by adding different metal cations such as Cd^{2+}, Co^{2+}, Zn^{2+}, Cu^{2+}, Ni^{2+}, Pb^{2+}, Mn^{2+}, Fe^{2+}, and Sn^{2+} into as-synthesized gelator (H_4L) in DMF (Figure 3.1). It can be noticeable that among these metal cations, specifically $Cu(OAc)_2$ was capable to form a gel with gelator H_4L. The morphological characteristics of the synthesized metallogel were investigated by the SEM, TEM, and AFM analysis.

3.7.1 UV-vis study

A UV-vis absorption spectroscopy investigation showed the complexation behaviour of gelator with Cu(II) in DMF. As shown in **Figure 3.2**, a UV-vis titration experiment was performed between gelator and Cu(II) metal ion by varying metal-gelator ratio. The UV-vis spectrum of the gelator exhibited two sharp bands at 281 nm and 290 nm, which may be due to π-π* transition. A less intense band at 322 nm corresponds to the n-π* transition[21]. The alternate band appeared at 281 nm, and 290 nm was due to unlike planarity of ligand[22], further multiple inclusions of $Cu(OAc)_2$ ($1x10^{-3}$M, DMF 25°C) to this solution, a substantial change was observed that vanishing of a band at 322 nm and new peak give the impression at 380 nm, specify the Cu^{+2} formed a complex with gelator[22] and the shift of wavelength (Δλ= 62 nm), with the origin of an isosbestic point at 342 nm specifies the existence of equilibrium state throughout the complexation of gelator and Cu(II) ion. In the range of 1-1.2 equivalent of gelator/Cu(II), showed saturation point indicates the possibility of 1:1 co-ordination, which was further confirmed by Job's plot for [Cu(II)]/[Cu(II)]+[gelator] *vs* absorbance monitored at 380 nm.

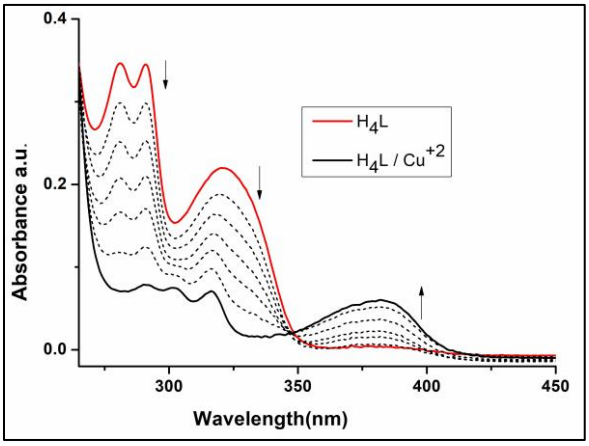

Figure. 3.2 UV-vis titration valuation of H_4L ($1x10^{-5}$ M, DMF, red line) with $Cu(OAc)_2$ ($1x10^{-3}$ M, DMF, black dotted lines).

3.7.2 FT-IR analysis

The gelator H_4L showed (**Figure 3.3 a**) a strong broadband in the region of 3200 cm^{-1} and a hump at 3430 cm^{-1}, which arises due to the vibration of secondary –NH groups and naphtholic/phenolic –OH groups, respectively[23]. The FT-IR spectra of the gelator also showed vibration at 1665 cm^{-1} and 1567 cm^{-1} due to the (>C=N) and (>C=O) vibrations respectively[18]. As shown in (**Figure 3.3 b**) the xerogel has strong broadband in the region of 3436 cm^{-1}; which suggests the -OH band of lattice/co-ordinated water molecules[18]. The synthesized xerogel did not show any band in the region of 3200 cm^{-1} (-NH); that attributed to the enol form in the complex[18]. The FT-IR spectra of xerogel >C=N, >C=O bands shifted to 1610 cm^{-1} ($\Delta\nu$=55) and 1505 cm^{-1} ($\Delta\nu$ = 62 cm^{-1}) from that of gelator, advocate the involvement of >C=N and >C=O in complexation[24]. Thus, it could be expected that co-ordination of Cu^{2+} with the synthesized gelator (H_4L) occurs through the O, N, O linkage.

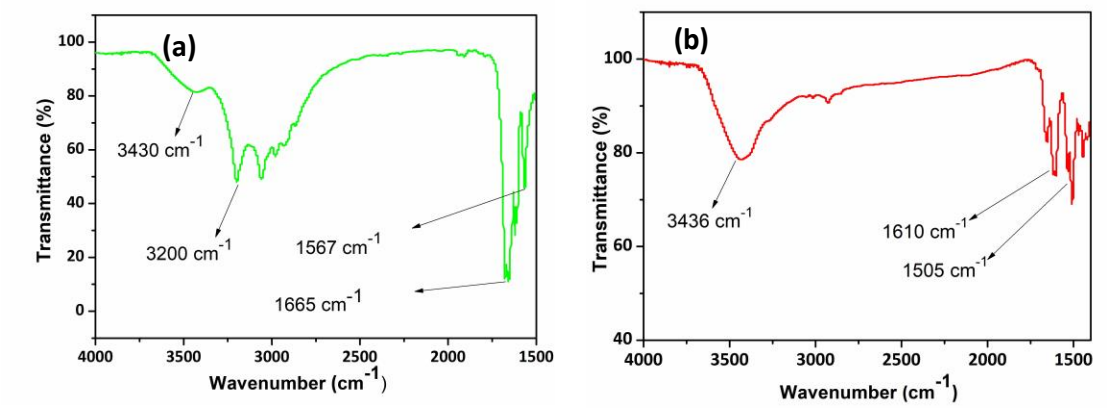

Figure. 3.3 FT-IR analysis of gelator (a) and xerogel (b) showing co-ordination of Cu^{2+} through O, N, O linkage.

3.7.3 Morphological study

The morphological characteristics of the synthesized metallogel were investigated by the FESEM, TEM, and AFM analysis. The microstructural pattern of supramolecular Cu-H_4L based metallogel explored by FESEM. The interconnected collection of thread-like nanofiber morphology of gel has an average size ~1 μm, as shown in **Figure 3.4(a)**. Morphological properties of the metallogel dictate the compactness of thin intertwined nanofibers. The network formation of nanofibers was confirmed by the TEM and AFM analysis of the metallogel, as revealed in **Figure 3.4(b)** and **Figure 3.4(c),** respectively. This result revealed the formation of an intermingled network of nanofibers along with an average diameter ~6 nm and several micrometre lengths. Supramolecular noncovalent interaction between the Cu(II)-source and the gelator H_4L in DMF could be effective for the self-assembly growth which offers the Cu(II) ion based stable metallogel.

Powder X-ray diffraction pattern of xerogel, formed using Cu-H_4L metallogel, in the 2θ range of 10^o to 90^o showed a common broad diffraction peak at 21.6° indicates the amorphous behaviour of the gel[25,26,27], as shown in **Figure 3.5**.

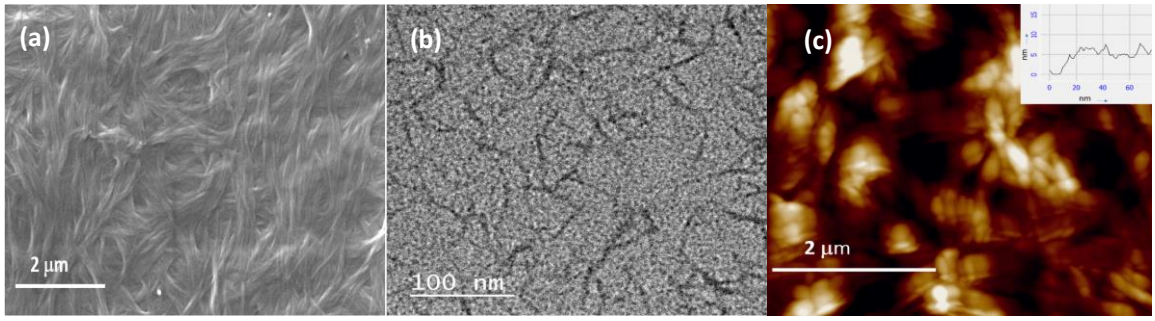

Figure. 3.4 (a) SEM picture of vacuum-dried metallogel, (b) and (c) TEM and AFM images of metallogel ($H_4L/Cu(OAc)_2$; ~10^{-3} M), respectively.

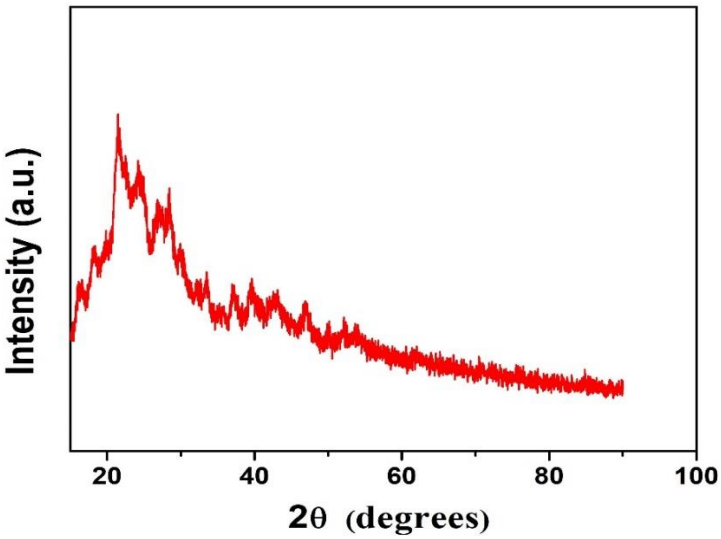

Figure 3.5 Powder X-ray diffraction pattern of xerogel, formed using Cu-H_4L metallogel.

Thermogravimetric analysis (TGA) is a substantial method to detect the thermal stability of a material, including polymers[28]. In this technique, a change in the weight of a sample is measured with respect to the increase in temperature. TGA measurement was carried out on

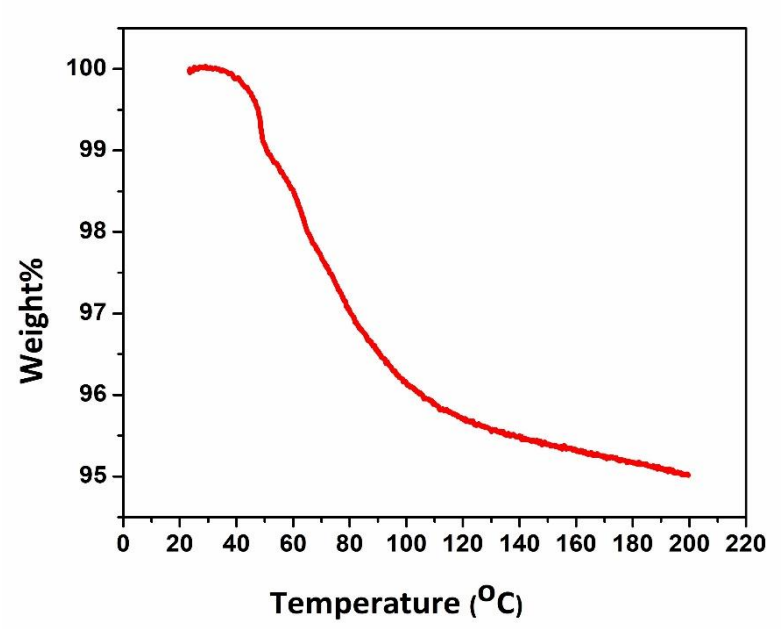

Figure 3.6 TGA curve of the xerogel form Cu (II)-H_4L metallogel.

15.8 mg of Cu (II)-H_4L xerogel at a heating rate of 10°C/min in a nitrogen atmosphere using a Thermogravimetric Analyzer (Instrument Model: TGA-50, Shimadzu (Asia Pacific) Pte Ltd). The continuous weight loss and temperature were analyzed thoroughly after recording; **(Figure 3.6)** the result showed that up to 200°C not as much weight loss was observed; this indicates the material thermal stability of gel when it is exposed to heat at 200°C.

The oxidation state of Cu was confirmed by X-ray photoelectron spectroscopy (XPS). The Cu XPS spectra was deconvoluted into two peaks Cu $2p_{3/2}$ and Cu $2p_{1/2}$ with corresponding binding energy 936.0 and 956.0 eV. The Cu $2p_{3/2}$ peak was further splitted into two peaks of Cu^+ and Cu^{2+} with corresponding energy 933.9 and 936.1 eV and two satellite peaks at 942.7 and 946.2 eV. The Cu 2p1/2 peak was deconvoluted into two peaks of Cu^+ and Cu^{2+} with corresponding energy 954.1 and 956.2 eV.[29] (**Figure 3.7**).

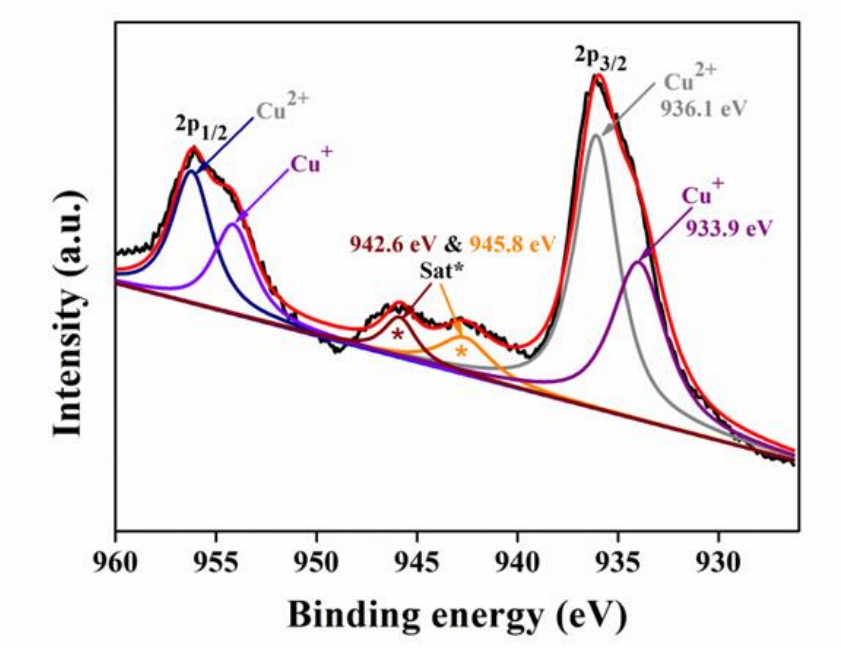

Figure. 3.7 Represents the high-resolution XPS spectrum of Cu 2p of synthesized Xerogel.

3.7.4 Mass spectral analysis

The Job's plot method (**Figure 3.8(a))** indicates the stoichiometric ratio of the complex formed during gelation between Cu^{2+} and gelator H_4L in DMF solvent is 1:1; under experimental condition. This was further confirmed by HR-MS spectral analysis of diluted metallogel. As shown in **Figure 3.8(b),** the molecular ion (m/z) peak spectrum was recorded by positive mode. A base peak was found for an isotopic abundance of gelator $[C_{18}H_{18}N_4O_4]$: 354.2, and its calculated base peak was observed at m/z 354.1. However, the base peak for diluted metallogel $[C_{18}H_{16}CuN_4O_4]^{-2}$ was found at m/z 415.2 and its estimated peak was at 415.1. Therefore, molecular ion abundance pattern of HR-MS spectra is smoothly matched with the calculated

peak. The molecular abundance pattern of metallogel well-matched with 1:1 proposed co-ordination mechanism between H_2L^{2-} and Cu^{2+} based on Job's plot, UV-vis study.

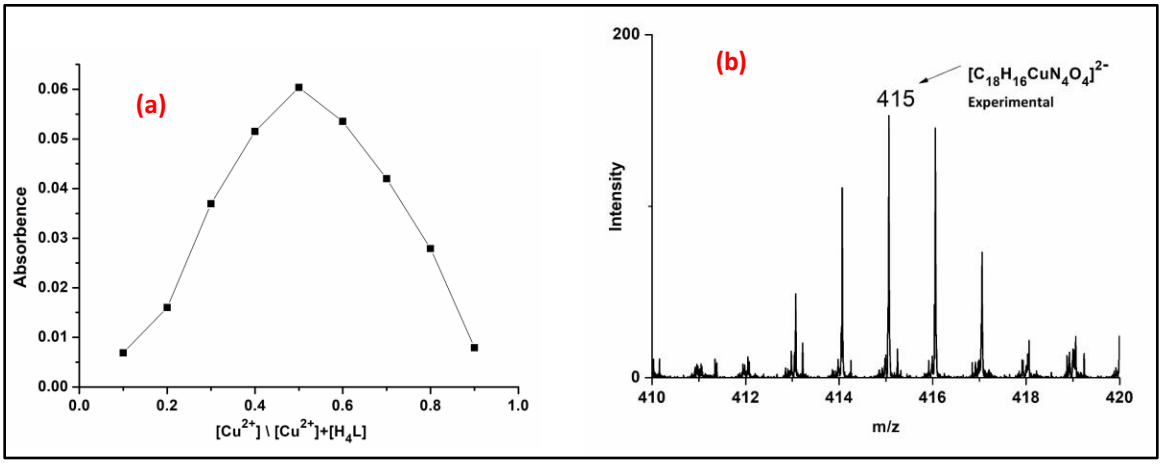

Figure. 3.8 (a) Represents Job's plot for [Cu(II)]/[Cu(II)]+[gelator] *vs* absorbance monitored at 380 nm. (b) HR-MS spectra of $[C_{18}H_{16}CuN_4O_4]$, represents the experimental isotopic abundance pattern for 1:1 H_4L vs Cu^{2+}.

3.7.5 Rheological analysis

A semi-solid nature with viscoelasticity of Cu based metallogel was confirmed by a rheological study such as angular frequency and strain sweep studies. The storage modulus (G') and loss modulus (G") measurement of gel is directly associated with the function of shear strain and shear stress, respectively at 25 ^{o}C and frequency of 10 rad.s^{-1}. In the viscoelastic region, G' of metallogel showed the stored energy in the system during the application of shear. For a liquid-like sample, G" indicates energy change during dissolution under the oscillatory stress[32]. The rheological experiment showed that G' of Cu-based metallogel was higher than that of G" by order ~1 of shear stress at the fixed concentration of the gel **(Figure 3.9)**. We have also observed that the value of shear stress of G' and G" intersect at point ~1.9 Pa, this point is gel destruction point, which is known as a gel-sol transition point. The operation of frequency sweep measurement was conducted between 0.1 to 100 rad.s^{-1}. The viscoelastic value of a gel in the range of 10^{-1}-10^{2} rad.s^{-1}, indicated that G' and G" value increases linearly with increasing applied frequency. This result exhibited the elastic nature of gel. As shown in **Figure 3.9**, it was observed that the value of G' > G", which indicates the retention of the structural property of Cu-H_4L metallogel.

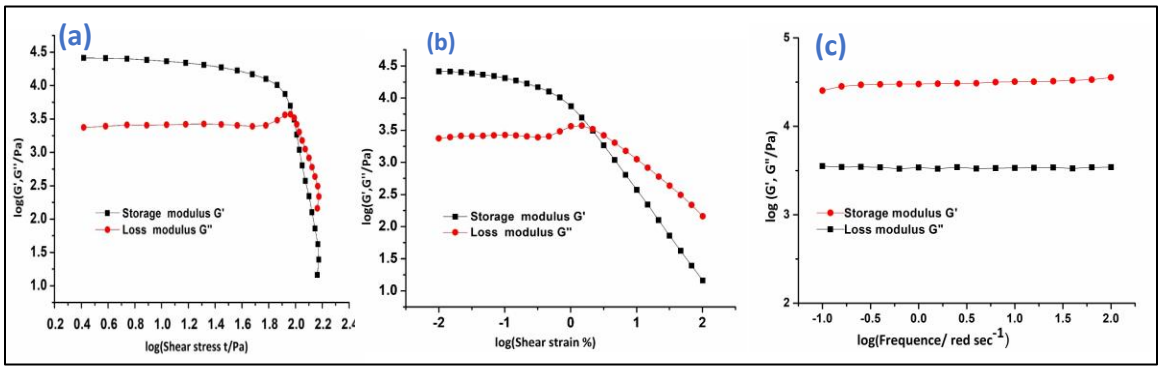

Figure. 3.9 (a) Dynamic shear stress against G" and G′, (b) dynamic oscillation Strain vs G" and G′, (c) frequency sweep measurements of G" and G′.

3.7.6 Optical characterization

The optical characteristics were probed by UV-vis spectroscopy. The UV-vis spectrum (solid-state) of thin film of Cu-H_4L metallogel was recorded between the range 250-600 nm. The calculation of the direct optical band gap of thin-film Cu-H_4L metallogel was performed using Tauc's equation[20,33].

$$(\alpha h\nu)^2 = A(h\nu - Eg) \quad (1)$$

where Eg, h, α and ν stand for optical bandgap, Planck's constant, absorption coefficient, and frequency of light, respectively. 'A' which is unity in an ideal case, is a constant. With the extrapolation of the linear region of the plot $(\alpha h\nu)^2$ vs. hν (**Figure 3.10**) to α = 0 absorptions, the direct optical band gap (Eg) was evaluated as 3.06 eV for Cu-H_4L metallogel

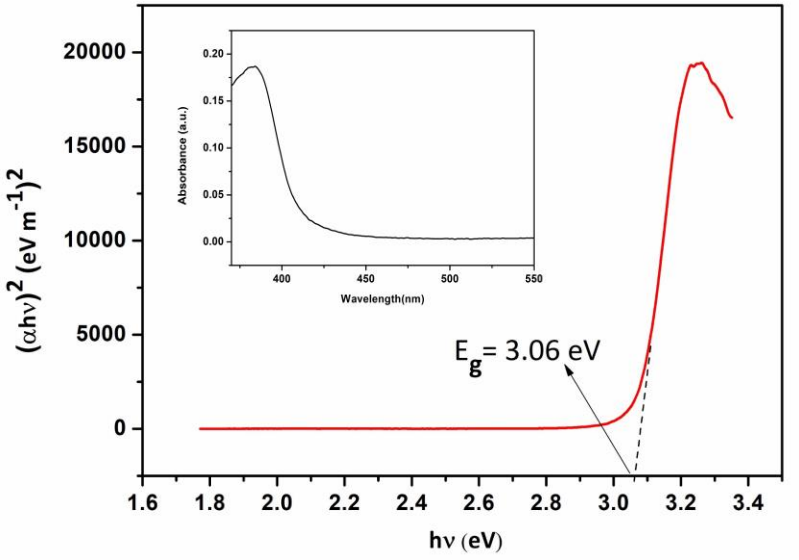

Figure. 3.10 The UV-vis absorption spectrum (inset) and Tauc's plot for Cu-H_4L.

3.8 Strategy of device fabrication

By using the above optical property of synthesized mettalogel, a Schottky diode was designed as shown in **Scheme 2**.

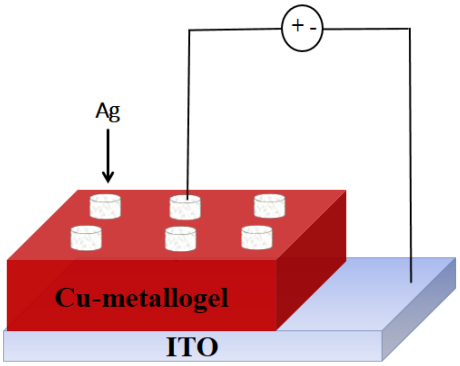

Figure.3.11 The image shows the fabrication of Schottky diode based on synthesized Cu-H_4L metallogel.

It is evident from the Tauc's plot analysis **(Figure 3.10)** that our synthesized organo-metallogel (Cu-H_4L) comes under semiconducting-range material. Hence, we have fabricated a metal (Ag)–Semiconductor (Cu-H_4L) (MS) junction based thin-film device and investigated the current-voltage (*I-V*) characteristics of the device. The (*I–V*) measurements of organo-metallogel (Cu-H_4L) based thin-film device were examined with the help of the semiconductor parameter analyser at a bias voltage from -2 V to +2 V at room temperature. *I–V* characteristics of fabricated devices have been examined, as shown in **Figure 3.12**. By using *I–V* characteristics of the Ag/Cu-H_4L based thin-film device, the interface between Ag/Cu-H_4L exhibits a nonlinear rectifying behaviour, which indicates the formation of a Schottky diode. The obtained current-voltage (*I-V*) characteristics of semiconductor gel at room temperature were further analyzed by assuming the standard thermionic theory and Cheung's equation[34,35,36] and calculated key parameter of the fabricated device. To analyze the I-V graph, we have first employed the following standard equation:

$$I = I_0 \exp\left(\frac{qV}{\acute{\eta}KT}\right)\left(1 - \exp\left(-\frac{-qV}{\acute{\eta}KT}\right)\right) \qquad (2)$$

$$I_0 = AA^* T^2 \exp\left(\frac{-q\phi_B}{KT}\right) \quad (3)$$

where I_0, q, K, T, V, A, η and A* represent reverse saturation current, electronic charge, Boltzmann constant, Temperature (K), Voltage, effective diode area, ideality factor and Richardson constant, respectively. The effective diode area was calculated as 0.0314 cm^2 and Richardson constant was considered as 32 A K^{-2} cm^{-2} for the Cu-H_4L Gel based devices.

We have also calculated the series resistance (Rs), ideality factor (ή) and barrier height (ϕ_B) by using following equations:

$$\frac{dV}{d(lnI)} = \left(\frac{\acute{\eta}KT}{q}\right) + IRs \quad (4)$$

$$\phi_B = \frac{KT}{q} ln\left(\frac{A^* T^2}{J_0}\right) \quad (5)$$

The estimated value of reverse saturation current was 3.80 x 10^{-6}A and value of the calculated Barrier height (ϕ_B), ideality factor (η), opening voltage (V) and series resistance (R_S) and for the synthesized complex-based SBD respectively are ~0.61 eV, ~3.0, ~0.5 volts ~65 Ω. For a better understanding of the charge transport phenomena in the fabricated device, we have analyzed the logarithmic scale I-V characteristics which are shown in **Figure 3.13**. it reveals that it can be divided into two slopes which have been defined as region-I and region-II. In the region-I, current follows linear behavior with voltage which refers to the ohmic regime. In the region-II, current follows nonlinear behavior with voltage and current is proportional to V^2. This refers to trap free space charge limited current (SCLC) region[37].

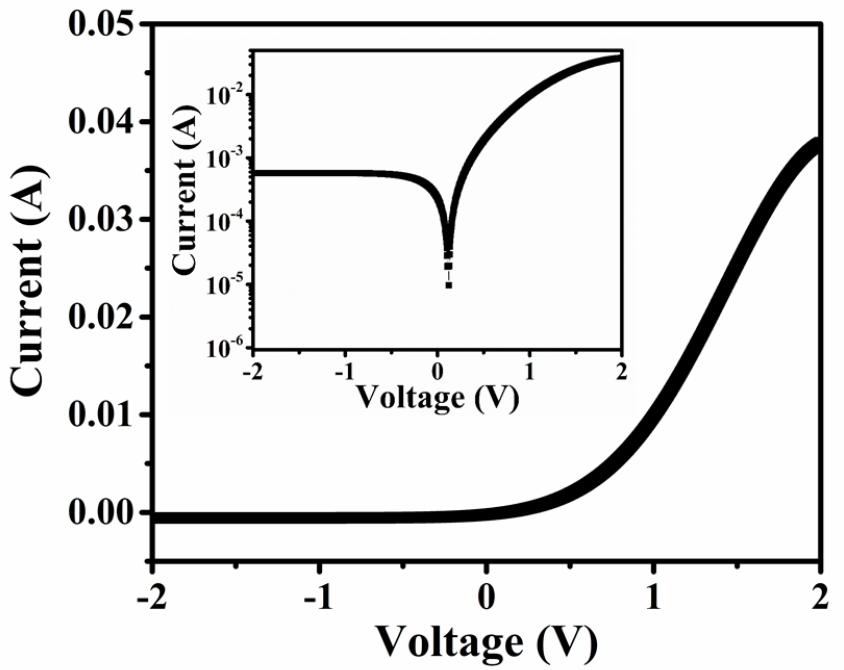

Figure 3.12 *I–V* characteristics graph for ITO/Cu-H_4L/Ag-based thin-film device

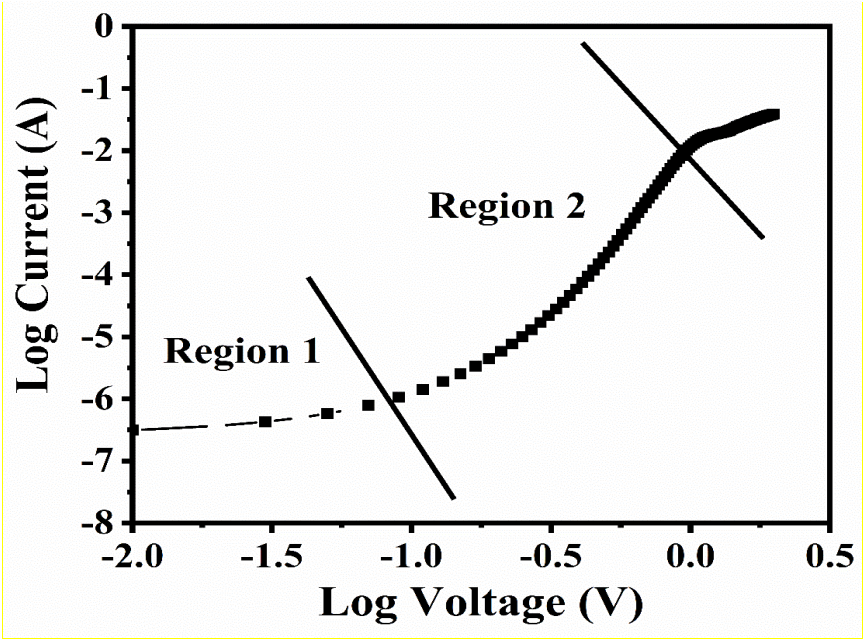

Figure 3.13 log I vs. log V curve for ITO/Cu-H_4L/Ag-based thin-film device.

Table 3.1. Comparison Table Showing Charge Transport Parameters of the Ag/Cu-H_4L device

Device name	**ON/OFF ratio**	**Series resistance (Ω)**	**Barrier height (eV)**	**Ideality factor**	**Reference**
Fe@MEA	375	13.9	0.72	1.33	[38]
$[Cd_4L_2(NCO)_6]_n$	12.44	5306	0.52	3.45	[39]
$C_{40}H_{34}Cu_2N_6O_{18}$	8.46	81.7	0.47	2.78	[40]
Au/CuO/P-Si/Al	-	410	0.79	1.58	[41]
Cu/ZnO	-	-	0.67	1.99	[42]
Ag/Cu-H_4L	**70**	**65**	**0.61**	**3.0**	**Present work**

3.9 Conclusion

Herein, we have developed a practical synthesis of new modular and functional metallogel, based on succinic acid-derivative and $Cu(OAc)_2$ in DMF. Gel phase material was confirmed by rheological experiments and also been established the mechanical stability of metallogel. Well-defined cross-linked nanofibers of supramolecular Cu^{2+} based metallogel were confirmed by SEM, TEM, and AFM analysis. The FT-IR, UV-vis, HR-MS and Job's plot established the mechanism of metallogel. The optical band-gap measurement of metallogel based on succinic acid-derived compound (H_4L) and $Cu(OAc)_2$, suggests the semiconducting nature of the metallogel. Additionally, we have fabricated an MS junction thin-film electronic device by Ag metal and semiconducting Cu-H_4L gel. The non-linear charge transportation of the device obtained from the *I–V* characteristic graph was confirmed the fabrication of the Schottky diode. Thus, the present study of ITO/Cu-H_4L/Ag advocates the future possibility of achieving supramolecular Cu^{2+} metallogel based electronic devices for advanced technology

3.10 Reference:

1 K. Gao, Z. Zhang, L. Ma, L. Chen, X. Chen, Y. Zhang and M. Zhang, *Giant*, 2020, **4**, 100034.

2 Y. X. Ye, W. L. Liu and B. H. Ye, *Catal. Commun.*, 2017, **89**, 100–105.

3 F. A. Denis, P. Hanarp, D. S. Sutherland and Y. F. Dufrêne, *Langmuir*, 2004, **20**, 9335–9339.

4 W. Zhang, Z. Wang, L. Tao, K. Duan, H. Wang, J. Zhang, X. Pan and Z. Huo, *J. Solid State Electrochem.*, 2019, 1563–1570.

5 S. Bhowal, A. Ghosh, S. P. Chowdhuri, R. Mondal and B. B. Das, *Dalt. Trans.*, 2018, **47**, 6557–6569.

6 G. Liu, J. Sheng, W. L. Teo, G. Yang, H. Wu, Y. Li and Y. Zhao, *J. Am. Chem. Soc.*, 2018, **140**, 16275–16283.

7 J. Jagur-Grodzinski, *Polym. Adv. Technol.*, 2010, **21**, 27–47.

8 A. Biswas, S. Mukhopadhyay, R. S. Singh, A. Kumar, N. K. Rana, B. Koch and D. S. Pandey, *ACS Omega*, 2018, **3**, 5417–5425.

9 N. Malviya, C. Sonkar, R. Ganguly, D. Bhattacherjee, K. P. Bhabak and S. Mukhopadhyay, *ACS Appl. Mater. Interfaces*, 2019, **11**, 47606–47618.

10 V. Van Tran, D. Park and Y. C. Lee, *Environ. Sci. Pollut. Res.*, 2018, **25**, 24569–24599.

11 Q. Lin, T. T. Lu, X. Zhu, B. Sun, Q. P. Yang, T. B. Wei and Y. M. Zhang, *Chem. Commun.*, 2015, **51**, 1635–1638.

12 S. Dhibar, A. Dey, S. Majumdar, A. Dey, P. P. Ray and B. Dey, *Ind. Eng. Chem. Res.*, 2020, **59**, 5466–5473.

13 S. Saha, E. M. Schön, C. Cativiela, D. Díaz Díaz and R. Banerjee, *Chem. - A Eur. J.*,

2013, **19**, 9562–9568.

14 S. Ganta and D. K. Chand, *Inorg. Chem.*, 2018, **57**, 3634–3645.

15 S. Dhibar, A. Dey, A. Dey, S. Majumdar, D. Ghosh, P. P. Ray and B. Dey, *ACS Appl. Electron. Mater.*, 2019, **1**, 1899–1908.

16 R. Jana, A. Dey, M. Das, J. Datta, P. Das and P. P. Ray, *Appl. Surf. Sci.*, 2018, **452**, 155–164.

17 H. Sheng, S. Muthukumar, N. W. Emanetoglu and Y. Lu, *Appl. Phys. Lett.*, 2002, **80**, 2132–2134.

18 R. Borthakur, A. Kumar, A. Lemtur and R. A. Lal, *RSC Adv.*, 2013, **3**, 15139–15147.

19 R. K. Upadhyay, A. P. Singh, D. Upadhyay, S. Ratan, C. Kumar and S. Jit, *IEEE Photonics Technol. Lett.*, 2019, **31**, 1151–1154.

20 R. K. Upadhyay, A. P. Singh, D. Upadhyay, A. Kumar, C. Kumar and S. Jit, *IEEE Electron Device Lett.*, 2019, **40**, 1961–1964.

21 M. Sutradhar, T. Roy Barman, J. Kxlanke, M. G. B. Drew and E. Rentschler, *Polyhedron*, 2013, **53**, 48–55.

22 L. Wang, W. Qin, X. Tang, W. Dou and W. Liu, *J. Phys. Chem. A*, 2011, **115**, 1609–1616.

23 J. D. Ranford, J. J. Vittal and Y. M. Wang, *Inorg. Chem.*, 1998, **37**, 1226–1231.

24 M. Cametti, M. Cetina and Z. Džolić, *Dalt. Trans.*, 2015, **44**, 7223–7229.

25 X. Wang, T. He, L. Yang, H. Wu, R. Zhang, Z. Zhang, R. Shen, J. Xiang, Y. Zhang and C. Wei, *Nanoscale*, 2016, **8**, 6479–6483.

26 V. K. Singh, V. Singh, P. K. Yadav, S. Chandra, D. Bano, V. Kumar, B. Koch, M. Talat and S. H. Hasan, *New J. Chem.*, 2018, **42**, 12990–12997.

27 S. Chandra, V. K. Singh, P. K. Yadav, D. Bano, V. Kumar, V. K. Pandey, M. Talat and S. H. Hasan, *Anal. Chim. Acta*, 2019, **1054**, 145–156.

28 F. Rezaei, R. Yunus and N. A. Ibrahim, *Mater. Des.*, 2009, **30**, 260–263.

29 A. Upadhyay, A. Narula and C. P. Rao, *ACS Appl. Bio Mater.*, , DOI:10.1021/acsabm.0c01028.

30 D. Bano, S. Chandra, P. K. Yadav, V. K. Singh and S. H. Hasan, *J. Photochem. Photobiol. A Chem.*, 2020, **398**, 112558.

31 P. K. Yadav, V. K. Singh, S. Chandra, D. Bano, V. Kumar, M. Talat and S. H. Hasan, *ACS Biomater. Sci. Eng.*, 2019, **5**, 623–632.

32 S. Dhibar, A. Dey, R. Jana, A. Chatterjee, G. K. Das, P. P. Ray and B. Dey, *Dalt. Trans.*, 2019, **48**, 17388–17394.

33 S. Dhibar, A. Dey, D. Ghosh, S. Majumdar, A. Dey, P. P. Ray and B. Dey, *ACS Omega*, , DOI:10.1021/acsomega.9b03194.

34 S. K. Cheung and N. W. Cheung, *Appl. Phys. Lett.*, 1986, **49**, 85–87.

35 A. Dey, A. Layek, A. Roychowdhury, M. Das, J. Datta, S. Middya, D. Das and P. P. Ray, *RSC Adv.*, 2015, **5**, 36560–36567.

36 S. Dhibar, A. Dey, S. Majumdar, D. Ghosh, A. Mandal, P. P. Ray and B. Dey, *Dalt. Trans.*, 2018, **47**, 17412–17420.

37 A. Dey, S. Middya, R. Jana, M. Das, J. Datta, A. Layek and P. P. Ray, *J. Mater. Sci. Mater. Electron.*, 2016, **27**, 6325–6335.

38 S. Dhibar, R. Jana, P. P. Ray and B. Dey, *J. Mol. Liq.*, 2019, **289**, 111126.

39 P. Ghorai, A. Dey, P. Brandão, J. Ortega-Castro, A. Bauza, A. Frontera, P. P. Ray and A. Saha, *Dalt. Trans.*, 2017, **46**, 13531–13543.

40 A. Hossain, A. Dey, S. K. Seth, P. P. Ray, P. Ballester, R. G. Pritchard, J. Ortega-Castro, A. Frontera and S. Mukhopadhyay, *ACS Omega*, 2018, **3**, 9160–9171.

41 S. Çetinkaya, H. A. Çetinkara, F. Bayansal and S. Kahraman, *Sci. World J.*, , DOI:10.1155/2013/126982.

42 A. Khan, M. Hussain, M. A. Abbasi, Z. H. Ibupoto, O. Nur and M. Willander, *Semicond. Sci. Technol.*, , DOI:10.1088/0268-1242/28/12/125006.